








Low-rank Green's function representations applied to dynamical mean-field theory

Nan Sheng ^{1,2,*}, Alexander Hampel ², Sophie Beck ², Olivier Parcollet ^{2,3}, Nils Wentzell ²,
Jason Kaye ^{2,4,†} and Kun Chen ^{2,‡}

¹*Department of Chemistry, University of Chicago, 5735 S Ellis Ave, Chicago, Illinois 60637, USA*

²*Center for Computational Quantum Physics, Flatiron Institute, 162 5th Avenue, New York, New York 10010, USA*

³*Université Paris-Saclay, CNRS, CEA, Institut de Physique Théorique, Gif-sur-Yvette 91191, France*

⁴*Center for Computational Mathematics, Flatiron Institute, 162 5th Avenue, New York, New York 10010, USA*



(Received 1 February 2023; accepted 26 April 2023; published 13 June 2023)

Several recent works have introduced highly compact representations of single-particle Green's functions in the imaginary time and Matsubara frequency domains, as well as efficient interpolation grids used to recover the representations. In particular, the intermediate representation with sparse sampling and the discrete Lehmann representation (DLR) make use of low rank compression techniques to obtain optimal approximations with controllable accuracy. We consider the use of the DLR in dynamical mean-field theory (DMFT) calculations, and in particular show that the standard full Matsubara frequency grid can be replaced by the compact grid of DLR Matsubara frequency nodes. We test the performance of the method for a DMFT calculation of Sr_2RuO_4 at temperature 50 K using a continuous-time quantum Monte Carlo impurity solver, and demonstrate that Matsubara frequency quantities can be represented on a grid of only 36 nodes with no reduction in accuracy, or increase in the number of self-consistent iterations, despite the presence of significant Monte Carlo noise.

DOI: [10.1103/PhysRevB.107.245123](https://doi.org/10.1103/PhysRevB.107.245123)

I. INTRODUCTION

In the past several decades, dynamical mean-field theory (DMFT) [1] has become a standard method for studying interacting fermionic lattice problems. In combination with first-principles methods [2,3], it has been widely adopted to calculate properties of strongly correlated materials. In such DMFT calculations of real materials, the low-temperature regime is of particular importance, as numerous experimental examples show: the critical temperature T_C for superconductivity in Sr_2RuO_4 is as low as approximately $1.5 \text{ K} \approx 10^{-4} \text{ eV}$ [4]; the magnetic ordering in double-perovskite iridates sets is below 2 K [5]. In these cases, the ordering temperature energy scale differs by about five orders of magnitude from the high-energy cutoff of approximately 10 eV.

The single-particle Green's function, a central quantity in DMFT, is often calculated in the imaginary time or Matsubara frequency domain. The standard representation on an equispaced grid in imaginary time, or on Matsubara frequencies up to a cutoff, is low-order accurate, and requires

$$N = \mathcal{O}(\beta\omega_{\max}) \quad (1)$$

degrees of freedom. Here, β is the inverse temperature, and ω_{\max} is the high energy cutoff of the spectral function (i.e., $\rho(\omega) = 0$ outside $[-\omega_{\max}, \omega_{\max}]$). In typical DMFT calculations, computing the local Green's function requires a possibly expensive Brillouin zone (BZ) integration for each

Matsubara frequency grid point and each iteration of a self-consistency loop determining the chemical potential. This cost can become substantial as the temperature is decreased.

A significant research effort has recently focused on developing compact and generic representations of imaginary time and Matsubara frequency Green's functions, beginning with orthogonal polynomial bases [6–9] and adaptive grid representations in imaginary time [7,10]. More recently, optimized basis sets obtained from low-rank compression of the Lehmann integral representation have been developed, along with associated stable interpolation grids allowing recovery of Green's functions from a small number of samples in either the imaginary time or Matsubara frequency domains. This began with the introduction of the orthogonal intermediate representation (IR) basis [11,12]. Interpolation grids for the IR were later developed using the sparse sampling method [13], and the related minimax isometry method [14] was developed to generate efficient grids for Matsubara frequency summation. Recently, some of the authors introduced the discrete Lehmann representation (DLR) [15], which uses a nonorthogonal but explicit basis of exponentials, with associated DLR interpolation grids. Both the IR and DLR bases, and their interpolation grids, contain only

$$N = \mathcal{O}(\log(\beta\omega_{\max}) \log(\epsilon^{-1})) \quad (2)$$

degrees of freedom, with ϵ a user-provided error tolerance. They therefore yield exceptionally compact representations with controllable, high-order accuracy. Fortran, Python, and Julia libraries are available for both the IR with sparse sampling [16] and the DLR [17]. Low-rank Green's function representations have been used to solve self-consistent diagrammatic equations in a variety of applications, including the

*nansheng@uchicago.edu

†jkaye@flatironinstitute.org

‡kunchen@flatironinstitute.org

SYK model [15,17,18], the self-consistent finite temperature GW method [13,19], Eliashberg-type equations for superconductivity [20–23], and Bethe-Salpeter-type equations for Hubbard models [24].

In this work we investigate the applicability and robustness of the DLR in self-consistent DMFT calculations. Specifically, we replace the standard Matsubara frequency grid with the compact DLR grid in the calculation of the local Green's function and all subsequent expressions in the DMFT equations. We find that this method is stable, even in the presence of noisy Green's function data as obtained from continuous-time quantum Monte Carlo (CTQMC) impurity solvers, and that neither the convergence nor the accuracy of self-consistent iteration is compromised. We demonstrate a reduction in computational effort and memory required to calculate the local Green's function by over two orders of magnitude for the correlated Hund's metal Sr_2RuO_4 at $T = 50$ K. Although the expensive solution of the impurity problem remains a barrier in many DMFT calculations, our approach therefore dramatically reduces the other significant cost in the DMFT loop, and leads to a more automated procedure.

II. BACKGROUND

A. The dynamical mean-field theory loop

We briefly outline the DMFT equations, and refer the reader to Refs. [1,2] for a more comprehensive overview. The central quantity of interest is the local Green's function

$$G_{\text{loc}}(i\nu_n) = \int_{\text{BZ}} \frac{d\mathbf{k}}{V_{\text{BZ}}} [i\nu_n - \epsilon_{\mathbf{k}} + \mu - \Sigma(\mathbf{k}, i\nu_n)]^{-1}. \quad (3)$$

Here $i\nu_n = i(2n+1)\pi/\beta$ is the Matsubara frequency variable (for fermionic Green's functions), $\epsilon_{\mathbf{k}}$ is the noninteracting lattice Hamiltonian, μ is the chemical potential, $\Sigma(\mathbf{k}, i\nu_n)$ is the lattice self-energy, and V_{BZ} is the volume of the BZ. The chemical potential can be computed self-consistently in each DMFT iteration in order to maintain the correct particle density. In DMFT, the self-energy is approximated as a local quantity, and is computed from the Green's function $G_{\text{imp}}(i\nu_n)$ of an effective impurity problem via the Dyson equation

$$\Sigma(\mathbf{k}, i\nu_n) \approx \Sigma_{\text{imp}}(i\nu_n) = \mathcal{G}_0^{-1}(i\nu_n) - G_{\text{imp}}^{-1}(i\nu_n). \quad (4)$$

Here, the effective noninteracting bath is represented by the Weiss mean-field

$$\mathcal{G}_0^{-1}(i\nu_n) = G_{\text{loc}}^{-1}(i\nu_n) + \Sigma_{\text{imp}}(i\nu_n), \quad (5)$$

obtained from the local Green's function Eq. (3). The local Green's function is obtained self-consistently, and convergence is reached when $G_{\text{loc}} = G_{\text{imp}}$. For concreteness, we focus in this paper on the continuous-time hybridization expansion (CTHYB) impurity solver [25], in which the impurity problem is defined through the local noninteracting Hamiltonian

$$H_{0,\text{loc}} = \int_{\text{BZ}} \frac{d\mathbf{k}}{V_{\text{BZ}}} \epsilon_{\mathbf{k}} - \mu \quad (6)$$

and the Matsubara frequency hybridization function

$$\Delta(i\nu_n) = i\nu_n - \mathcal{G}_0^{-1}(i\nu_n) - H_{0,\text{loc}}, \quad (7)$$

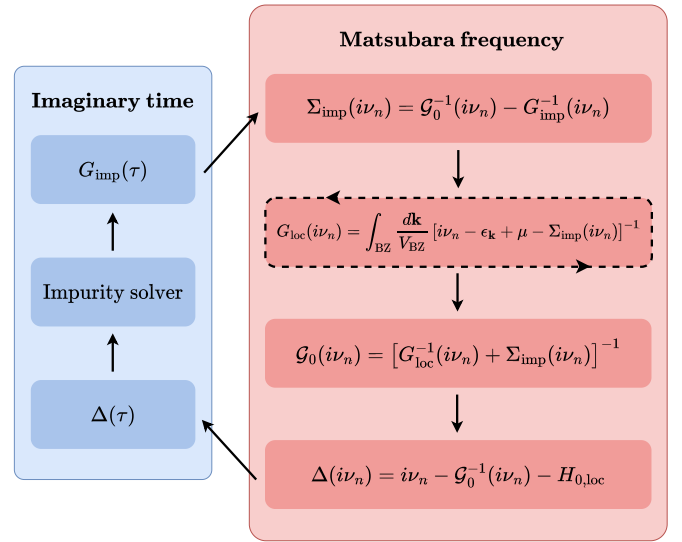


FIG. 1. The steps of the DMFT loop. The arrows around the formula for G_{loc} indicate that this quantity is computed self-consistently with the chemical potential to maintain the correct particle density. Our approach improves the efficiency of the DMFT loop by making two simple changes compared with the standard algorithm: (1) All operations in the Matsubara frequency domain are carried out only at the DLR nodes $\nu_n = \nu_{n_k}$, rather than the full Matsubara frequency grid, and (2) the imaginary time hybridization function $\Delta(\tau)$ is obtained from the computed values $\Delta(i\nu_n)$ by forming a DLR expansion and obtaining its Fourier transform analytically.

or its Fourier transform $\Delta(\tau)$ to the imaginary time domain. We emphasize, however, that compact representations of the type used here are in principle equally applicable for other types of impurity solvers.

The DMFT loop, outlined above, is summarized in Fig. 1. Although the solution of the impurity problem is often the most computationally intensive and technical step in the DMFT loop, it is outside the scope of our current discussion. Rather, we focus on the calculation of $G_{\text{loc}}(i\nu_n)$, which requires the evaluation of a BZ integral for each Matsubara frequency grid point $i\nu_n$. In typical calculations all Matsubara frequency points are used up to a cutoff $\mathcal{O}(\omega_{\text{max}})$ [yielding $\mathcal{O}(\beta\omega_{\text{max}})$ points in total], in order to capture the effective energy scales of the system. We demonstrate here that the number of Matsubara frequency points at which $G_{\text{loc}}(i\nu_n)$ must be computed can be dramatically reduced.

B. Discrete Lehmann representation and compact Matsubara frequency grids

The DLR method provides a compact, explicit basis for Matsubara Green's functions and self-energies, along with associated interpolation grids. We give a brief review of these concepts here, and refer to Ref. [15] for a detailed presentation and analysis.

Each Matsubara Green's function $G(i\nu_n)$ has a spectral Lehmann representation

$$G(i\nu_n) = - \int_{-\infty}^{\infty} K(i\nu_n, \omega) \rho(\omega) d\omega, \quad (8)$$

where $\rho(\omega)$ is the spectral function, and the analytic continuation kernel K is given in the fermionic case by

$$K(iv_n, \omega) \equiv (\omega - iv_n)^{-1}. \quad (9)$$

In most practical applications, ρ is unknown, but $G(iv_n)$ can either be sampled directly or obtained from samples of the imaginary time Green's function $G(\tau)$. We assume ρ can be truncated beyond a frequency cutoff $|\omega| = \omega_{\max}$. Defining the dimensionless parameter

$$\Lambda \equiv \beta\omega_{\max},$$

and nondimensionalizing variables by $v_n \leftarrow \beta v_n$ and $\omega \leftarrow \beta\omega$, we obtain the truncated Lehmann representation

$$G(iv_n) = - \int_{-\Lambda}^{\Lambda} K(iv_n, \omega) \rho(\omega) d\omega, \quad (10)$$

where v_n is given as above with $\beta = 1$, and the arguments of G, ρ have been suitably rescaled.

It can be shown that the kernel of this integral representation $K(iv_n, \omega)$ has super-exponentially decaying singular values [11,12]. This low-rank structure is indicative of the well-known ill conditioning of analytic continuation from the Matsubara Green's function to the spectral function on the real frequency axis [26]. However, it is advantageous for the representation of Matsubara Green's functions themselves, implying that $K(iv_n, \omega)$ can be approximated for any $\omega \in [-\Lambda, \Lambda]$ as a linear combination of a small number of basis functions. In particular, the DLR approach uses frequency samples of the kernel itself as basis functions:

$$K(iv_n, \omega) \approx \sum_{l=1}^r K(iv_n, \omega_l) \pi_l(\omega). \quad (11)$$

The r DLR frequencies ω_l can be selected automatically by the pivoted Gram-Schmidt algorithm such that the approximation in Eq. (11) is numerically stable, and accurate to a user-provided error tolerance [27]. Substitution of Eq. (11) into Eq. (10) demonstrates the existence of an expansion of an arbitrary Matsubara Green's function in the basis $K(iv_n, \omega_l)$:

$$G(iv_n) \approx \sum_{l=1}^r K(iv_n, \omega_l) \widehat{g}_l, \quad (12)$$

with $\widehat{g}_l = - \int_{-\Lambda}^{\Lambda} \pi_l(\omega) \rho(\omega) d\omega$.

The rapid decay of the singular values of K implies the scaling $r = \mathcal{O}(\log(\Lambda) \log(\varepsilon^{-1}))$, yielding exceptionally compact expansions at high accuracies and low temperatures. For example, Matsubara Green's functions with $\Lambda = 100$ can be represented to six-digit accuracy by fewer than 20 basis functions; with $\Lambda = 10^4$ to six-digit accuracy by fewer than 50 basis functions; and with $\Lambda = 10^6$ to 10-digit accuracy by fewer than 120 basis functions. By contrast, in a typical calculation, for example with $\beta = 1000 \text{ eV}^{-1}$ and $\omega_{\max} = 10 \text{ eV}$ ($\Lambda = 10^4$), one would typically require on the order of tens of thousands of Matsubara frequencies. We emphasize that given Λ and ε , the representation is universal; that is, independent of the specific structure of the spectral function ρ characterizing the Green's function, which is already taken into account by the automatic compression of the kernel K .

Since ρ is typically not known and the DLR coefficients \widehat{g}_l cannot be computed directly, they can in practice be recovered by fitting, or by interpolation at a collection of r DLR Matsubara frequency nodes $\{iv_{n_k}\}_{k=1}^r$ [15]. These nodes can be obtained automatically, using a process similar to that used to obtain the DLR frequencies, to ensure stable interpolation. Thus, a Green's function G can be characterized, to within a controllable error, by its values $G(iv_{n_k})$ at the DLR nodes.

The Fourier transform of Eq. (12) yields an imaginary time representation

$$G(\tau) \approx \sum_{l=1}^r K(\tau, \omega_l) \widehat{g}_l, \quad (13)$$

with

$$K(\tau, \omega) \equiv \frac{e^{-\omega\tau}}{1 + e^{-\omega}}$$

in the transformed variables $\tau \leftarrow \tau/\beta$, $\omega \leftarrow \beta\omega$. As for the Matsubara frequency expansion, $G(\tau)$ can either be recovered by least squares fitting, or by interpolation at a collection of automatically selected DLR imaginary time nodes $\{\tau_k\}_{k=1}^r$. We note that the DLR interpolation procedure is similar to the method of sparse sampling used in conjunction with the IR basis, in which interpolation nodes are selected based on the extrema of the highest degree IR basis function [13].

III. RESTRICTION TO COMPACT MATSUBARA FREQUENCY GRID

We propose the following procedure to improve the efficiency of the DMFT loop: Given the self-energy Σ_{imp} , the local Green's function G_{loc} is evaluated only at the r DLR Matsubara frequency nodes $\{iv_{n_k}\}_{k=1}^r$, as are the Weiss mean-field \mathcal{G}_0 from Eq. (5) and the hybridization function Δ from Eq. (7). At this point, the DLR expansion of $\Delta(iv_n)$ is formed by interpolation from its values at the DLR nodes using the representation in Eq. (12), with G replaced by Δ . $\Delta(\tau)$ is then given analytically by a DLR expansion in imaginary time, as in Eq. (13). The rest of the DMFT procedure can be carried out without modification.

The primary purpose of this paper is to verify that systematic or statistical error generated by the quantum impurity solver does not destabilize our proposed procedure. Although this question depends on the specific choice of impurity solver, we carry out tests using the most popular solver, CTQMC. We show in the next section that the interpolation procedure is stable to Monte Carlo noise, and that the convergence of the DMFT loop is not affected by the reduction of the Matsubara frequency grid.

IV. NUMERICAL EXAMPLE: STRONTIUM RUTHENATE

We demonstrate our procedure using the correlated Hund's metal Sr_2RuO_4 [28] at low T . We compute the electronic structure using the planewave-based QUANTUM ESPRESSO package [29] using the standard Perdew–Burke–Ernzerhof exchange–correlation functional, and scalar-relativistic ultrasoft pseudopotentials [30]. After structural optimization on a $12 \times 12 \times 12$ Monkhorst-Pack grid, we obtain lattice parameters that correspond to $a = 3.880 \text{ \AA}$ and

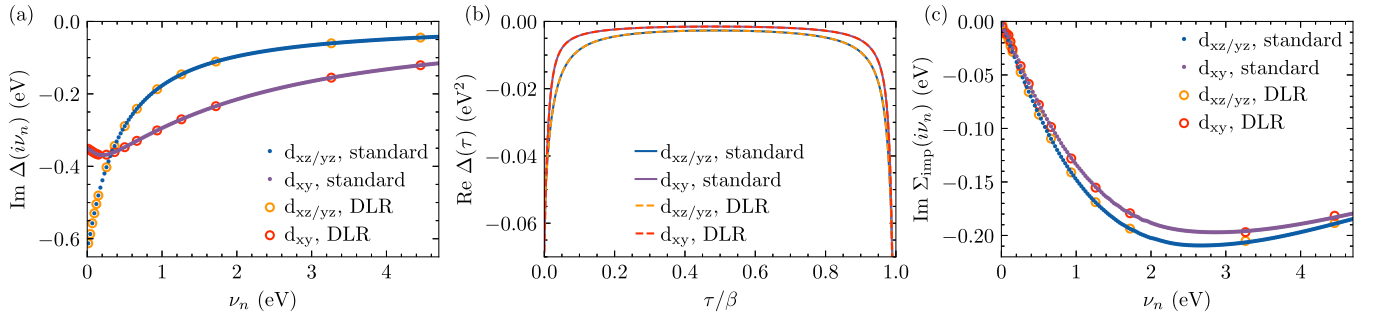


FIG. 2. Orbital-resolved hybridization function Δ and self-energy Σ_{imp} of the three t_{2g} orbitals during the first iteration of the DMFT loop for the Sr_2RuO_4 example, demonstrating the use of the DLR procedure. (a) $\Delta(iv_n)$ (from initial guess with zero self-energy) given by Eq. (7). (b) $\Delta(\tau)$ obtained using the standard method, i.e., asymptotic expansion and discrete Fourier transform, and DLR interpolation from the values $\Delta(iv_{n_k})$. (c) $\Sigma_{\text{imp}}(iv_n)$ calculated via the Dyson equation after the impurity problem is solved, with the hybridization functions obtained using both methods. To suppress QMC noise, an asymptotic expansion is fit to the tail above $\nu_n = 2$ eV. In the DLR approach, all Matsubara frequency quantities are obtained only at the DLR nodes iv_{n_k} (with the parameters $\omega_{\text{max}} = 12$ eV and $\epsilon = 10^{-6}$ eV $^{-1}$), which are indicated in (a) and (c).

$c = 12.887$ Å in the conventional unit cell [space group I4/mmm (139)]. The primitive unit cell contains one ruthenium site with a partially filled t_{2g} shell for which we construct three maximally localized Wannier functions [31], representing the degenerate d_{xz}/d_{yz} orbitals and the d_{xy} orbital. We recompute the Hamiltonian on a $40 \times 40 \times 40$ k -point grid using Wannier interpolation in order to compute the BZ integrals in Eq. (3) by equispaced integration. We add a local rotationally invariant Hubbard-Kanamori interaction with $U = 2.3$ eV and $J = 0.4$ eV [28]. The impurity problem is solved using TRIQS/CTHYB [25] in the TRIQS library [32]. To address the well-known numerical instability of computing the self-energy via the Dyson equation in Eq. (4) in the presence of quantum Monte Carlo (QMC) noise, we replace this formula at high frequencies with an asymptotic expansion. This expansion is given by a polynomial in $(iv_n)^{-1}$, fit to Σ_{imp} in a window in which the QMC noise is sufficiently small so that Eq. (4) is valid.

The DMFT calculation is implemented using the TRIQS library [32], and the Python library `pydlr` provided by `libdlr` [17,33] is used for DLR calculations. We solve the DMFT equations at $\beta = 232$ eV $^{-1}$, which corresponds to $T = 50$ K. We note that the DLR scheme is equally applicable at much lower temperatures, and we are hindered only by the sign problem of the Monte Carlo impurity solver used in our calculations. At this temperature, without the DLR, approximately 12 000 Matsubara frequency nodes are required to adequately capture the slowly-decaying tail of the Green's functions to allow for accurate Fourier transforms. More specifically, in the TRIQS library, the Fourier transform $\Delta(\tau)$ of $\Delta(iv_n)$ is obtained by the following procedure: (1) fit an asymptotic expansion in inverse powers of iv_n to $\Delta(iv_n)$, (2) Fourier transform this asymptotic expansion analytically, (3) Fourier transform the difference between $\Delta(iv_n)$ and its asymptotic expansion, which is rapidly decaying, by a discrete Fourier transform on the Matsubara frequency grid, and add the results. We note that since the asymptotic expansion is not valid until $n = \mathcal{O}(\Lambda)$, and one must fit from a window well within the tail region, a large number of Matsubara frequencies is typically needed in this procedure.

Choosing $\omega_{\text{max}} = 12$ eV and $\epsilon = 10^{-6}$ eV $^{-1}$, the number of DLR basis functions and Matsubara frequency nodes is $r = 36$, reducing the number of BZ integrals required to calculate G_{loc} in Eq. (3) by a factor of over 300 in this case. While it may be possible to further optimize the number of Matsubara frequencies used in the standard approach, our method nevertheless represents a reduction from $\mathcal{O}(\Lambda)$ nodes, with typically a large prefactor, to $\mathcal{O}(\log \Lambda)$ nodes. Furthermore, it avoids the complicated Fourier transform procedure used with the standard Matsubara frequency grid, since $\Delta(\tau)$ is obtained from the DLR expansion of $\Delta(iv_n)$ by analytical Fourier transform.

Figure 2 shows the first iteration of the DMFT loop comparing the hybridization function and the self-energy obtained using the standard method and the DLR approach (shown in markers/dashed lines and solid lines, respectively). In our scheme, we first compute G_{loc} , \mathcal{G}_0 , and Δ at the DLR nodes $iv_n = iv_{n_k}$, using zero self-energy as an initial guess in Eq. (3). The hybridization function $\Delta(iv_n)$ is shown in Fig. 2(a) on the full Matsubara frequency grid, as used in the standard method, with the DLR nodes used in our method indicated. The DLR expansion of $\Delta(\tau)$ obtained from interpolation at these nodes and analytical Fourier transform is shown in Fig. 2(b). Since no Monte Carlo noise has been introduced at this stage, the

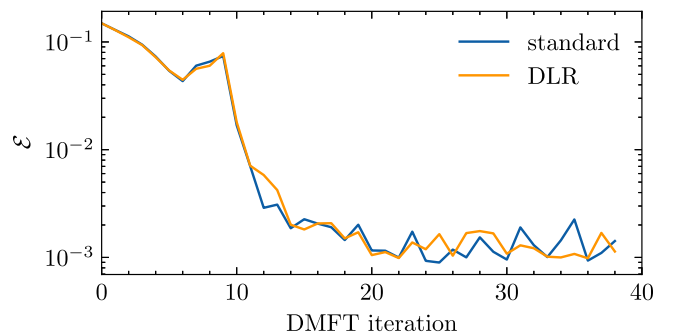


FIG. 3. Convergence of DMFT self-consistency for the Sr_2RuO_4 example using standard and DLR procedures, measured via the norm of the difference between G_{imp} and G_{loc} in τ [see Eq. (14)].

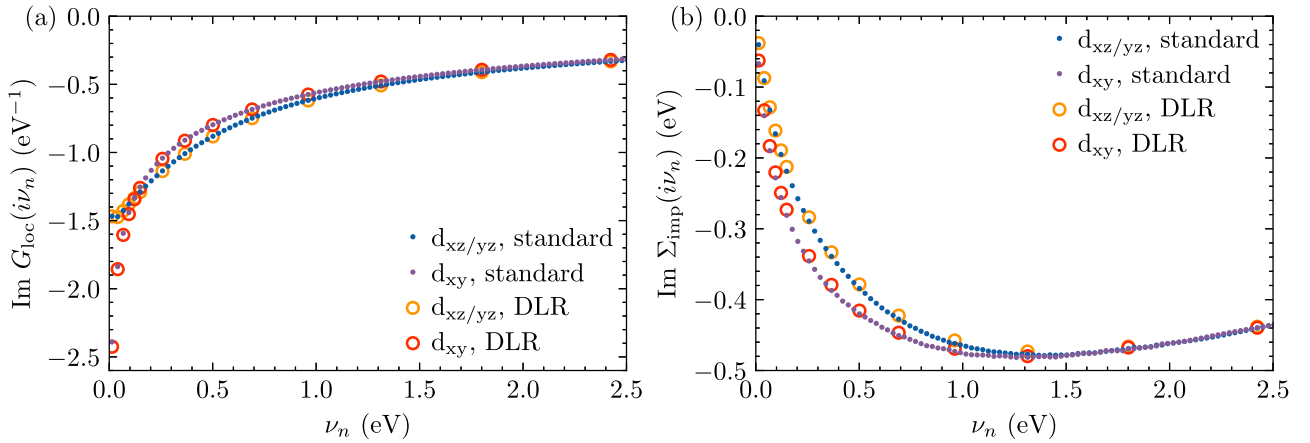


FIG. 4. Imaginary part of the orbitally-resolved (a) local Green's function, and (b) impurity self-energy in a low-frequency window for the Sr_2RuO_4 example, obtained using both the standard and DLR procedures. We show the converged results, obtained independently using the two methods. In the DLR procedure, Matsubara frequency quantities are obtained only at the indicated DLR nodes (with the parameters $\omega_{\text{max}} = 12 \text{ eV}$ and $\epsilon = 10^{-6} \text{ eV}^{-1}$).

DLR expansion of $\Delta(\tau)$ is correct to the DLR tolerance ϵ . We then solve the impurity problem using the DLR expansion of $\Delta(\tau)$ to obtain the impurity Green's function, and subsequently the self-energy $\Sigma(i\nu_n)$, shown in Fig. 2(c). We see that the self-energies obtained using the hybridization function obtained using the full grid DMFT procedure (shown at all Matsubara frequencies as dots) and the DLR procedure (shown at the DLR nodes as open circles) in the impurity solver agree to within the Monte Carlo noise level.

We next run the standard and modified DMFT loops until self-consistency. Convergence is measured by monitoring the quantity

$$\mathcal{E} = \sqrt{\frac{1}{\beta} \int_0^\beta d\tau \|G_{\text{imp}}(\tau) - G_{\text{loc}}(\tau)\|_F^2}, \quad (14)$$

where $\|\cdot\|_F$ indicates the Frobenius norm, and the normalization prevents a trivial scaling of the error with β , assuming a uniform distribution of Monte Carlo error. Figure 3 shows that the convergence behavior is nearly identical for the two approaches, with both reaching self-consistency after approximately 20 iterations. Finally, Fig. 4 shows $G_{\text{loc}}(i\nu_n)$

and $\Sigma_{\text{imp}}(i\nu_n)$ at convergence, demonstrating that the final results of the two calculations agree to within the Monte Carlo noise level.

V. CONCLUSION

Our proposed method improves the efficiency of the DMFT procedure by replacing the standard full Matsubara frequency grid with a highly compact grid compatible with interpolation using the DLR basis. We demonstrate the effectiveness of this approach for a DMFT calculation of Sr_2RuO_4 using CTQMC as the impurity solver. In general, our results suggest that the standard representations of quantities appearing in the DMFT loop can be replaced by much more efficient representations, such as the DLR, without incurring a penalty in accuracy or stability. We note that the same approach should be applicable to other impurity solvers, in particular fast approximate solvers used in real materials applications.

ACKNOWLEDGMENT

The Flatiron Institute is a division of the Simons Foundation.

-
- [1] A. Georges, G. Kotliar, W. Krauth, and M. J. Rozenberg, Dynamical mean-field theory of strongly correlated fermion systems and the limit of infinite dimensions, *Rev. Mod. Phys.* **68**, 13 (1996).
 - [2] G. Kotliar, S. Y. Savrasov, K. Haule, V. S. Oudovenko, O. Parcollet, and C. A. Marianetti, Electronic structure calculations with dynamical mean-field theory, *Rev. Mod. Phys.* **78**, 865 (2006).
 - [3] K. Held, Electronic structure calculations using dynamical mean field theory, *Adv. Phys.* **56**, 829 (2007).
 - [4] Y. Liu and Z.-Q. Mao, Unconventional superconductivity in Sr_2RuO_4 , *Phys. C: Supercond. Appl.* **514**, 339 (2015).
 - [5] J. Terzic, H. Zheng, F. Ye, H. D. Zhao, P. Schlottmann, L. E. De Long, S. J. Yuan, and G. Cao, Evidence for a low-temperature magnetic ground state in double-perovskite iridates with $\text{Ir}^{5+}(5d^4)$ ions, *Phys. Rev. B* **96**, 064436 (2017).
 - [6] L. Boehnke, H. Hafermann, M. Ferrero, F. Lechermann, and O. Parcollet, Orthogonal polynomial representation of imaginary-time Green's functions, *Phys. Rev. B* **84**, 075145 (2011).
 - [7] A. A. Kananenka, J. J. Phillips, and D. Zgid, Efficient temperature-dependent Green's functions methods for realistic systems: Compact grids for orthogonal polynomial transforms, *J. Chem. Theory Comput.* **12**, 564 (2016).
 - [8] E. Gull, S. Isakov, I. Krivenko, A. A. Rusakov, and D. Zgid, Chebyshev polynomial representation of imaginary-time response functions, *Phys. Rev. B* **98**, 075127 (2018).
 - [9] X. Dong, D. Zgid, E. Gull, and H. U. R. Strand, Legendre-spectral Dyson equation solver with

- super-exponential convergence, *J. Chem. Phys.* **152**, 134107 (2020).
- [10] W. Ku and A. G. Eguiluz, Band-Gap Problem in Semiconductors Revisited: Effects of Core States and Many-Body Self-Consistency, *Phys. Rev. Lett.* **89**, 126401 (2002).
- [11] H. Shinaoka, J. Otsuki, M. Ohzeki, and K. Yoshimi, Compressing Green's function using intermediate representation between imaginary-time and real-frequency domains, *Phys. Rev. B* **96**, 035147 (2017).
- [12] N. Chikano, J. Otsuki, and H. Shinaoka, Performance analysis of a physically constructed orthogonal representation of imaginary-time Green's function, *Phys. Rev. B* **98**, 035104 (2018).
- [13] J. Li, M. Wallerberger, N. Chikano, C.-N. Yeh, E. Gull, and H. Shinaoka, Sparse sampling approach to efficient ab initio calculations at finite temperature, *Phys. Rev. B* **101**, 035144 (2020).
- [14] M. Kaltak and G. Kresse, Minimax isometry method: A compressive sensing approach for Matsubara summation in many-body perturbation theory, *Phys. Rev. B* **101**, 205145 (2020).
- [15] J. Kaye, K. Chen, and O. Parcollet, Discrete Lehmann representation of imaginary time Green's functions, *Phys. Rev. B* **105**, 235115 (2022).
- [16] M. Wallerberger, S. Badr, S. Hoshino, S. Huber, F. Kakizawa, T. Koretsune, Y. Nagai, K. Nogaki, T. Nomoto, H. Mori, J. Otsuki, S. Ozaki, T. Plaikner, R. Sakurai, C. Vogel, N. Witt, K. Yoshimi, and H. Shinaoka, sparse-ir: Optimal compression and sparse sampling of many-body propagators, *SoftwareX* **21**, 101266 (2023).
- [17] J. Kaye, K. Chen, and H. U. R. Strand, libldr: Efficient imaginary time calculations using the discrete Lehmann representation, *Comput. Phys. Commun.* **280**, 108458 (2022).
- [18] J. Kaye and H. U. R. Strand, A fast time domain solver for the equilibrium Dyson equation, [arXiv:2110.06120](https://arxiv.org/abs/2110.06120).
- [19] C.-N. Yeh, S. Isakov, D. Zgid, and E. Gull, Fully self-consistent finite-temperature GW in Gaussian Bloch orbitals for solids, *Phys. Rev. B* **106**, 235104 (2022).
- [20] T. Wang, T. Nomoto, Y. Nomura, H. Shinaoka, J. Otsuki, T. Koretsune, and R. Arita, Efficient ab initio Migdal-Eliashberg calculation considering the retardation effect in phonon-mediated superconductors, *Phys. Rev. B* **102**, 134503 (2020).
- [21] X. Cai, T. Wang, N. V. Prokof'ev, B. V. Svistunov, and K. Chen, Superconductivity in the uniform electron gas: Irrelevance of the Kohn-Luttinger mechanism, *Phys. Rev. B* **106**, L220502 (2022).
- [22] T. Wang, X. Cai, K. Chen, B. V. Svistunov, and N. V. Prokof'ev, On the origin of Coulomb pseudopotential: Two wrongs make a right, [arXiv:2207.05238](https://arxiv.org/abs/2207.05238).
- [23] Y. Nagai and H. Shinaoka, Sparse modeling approach for quasiclassical theory of superconductivity, *J. Phys. Soc. Jpn.* **92**, 034703 (2023).
- [24] M. Wallerberger, H. Shinaoka, and A. Kauch, Solving the Bethe-Salpeter equation with exponential convergence, *Phys. Rev. Res.* **3**, 033168 (2021).
- [25] P. Seth, I. Krivenko, M. Ferrero, and O. Parcollet, TRIQS/CTHYB: A continuous-time quantum Monte Carlo hybridisation expansion solver for quantum impurity problems, *Comput. Phys. Commun.* **200**, 274 (2016).
- [26] R. N. Silver, D. S. Sivia, and J. E. Gubernatis, Maximum-entropy method for analytic continuation of quantum Monte Carlo data, *Phys. Rev. B* **41**, 2380 (1990).
- [27] H. Cheng, Z. Gimbutas, P.-G. Martinsson, and V. Rokhlin, On the compression of low rank matrices, *SIAM J. Sci. Comput.* **26**, 1389 (2005).
- [28] A. Georges, L. d. Medici, and J. Mravlje, Strong correlations from Hund's coupling, *Annu. Rev. Condens. Matter Phys.* **4**, 137 (2013).
- [29] P. Giannozzi, S. Baroni, N. Bonini, M. Calandra, R. Car, C. Cavazzoni, D. Ceresoli, G. L. Chiarotti, M. Cococcioni, I. Dabo, A. D. Corso, S. de Gironcoli, S. Fabris, G. Fratesi, R. Gebauer, U. Gerstmann, C. Gougoussis, A. Kokalj, M. Lazzeri, L. Martin-Samos *et al.*, Quantum ESPRESSO: a modular and open-source software project for quantum simulations of materials, *J. Phys.: Condens. Matter* **21**, 395502 (2009).
- [30] K. F. Garrity, J. W. Bennett, K. M. Rabe, and D. Vanderbilt, Pseudopotentials for high-throughput DFT calculations, *Comput. Mater. Sci.* **81**, 446 (2014).
- [31] A. A. Mostofi, J. R. Yates, Y.-S. Lee, I. Souza, D. Vanderbilt, and N. Marzari, wannier90: A tool for obtaining maximally-localised Wannier functions, *Comput. Phys. Commun.* **178**, 685 (2008).
- [32] O. Parcollet, M. Ferrero, T. Ayrál, H. Hafermann, I. Krivenko, L. Messio, and P. Seth, TRIQS: A toolbox for research on interacting quantum systems, *Comput. Phys. Commun.* **196**, 398 (2015).
- [33] J. Kaye and H. U. R. Strand, libldr v1.0.0 (2022), <https://github.com/jasonkaye/libldr>.